Transp Porous Med (2008) 74:293–309
DOI 10.1007/s11242-007-9198-0

Numerical Study of Natural Convection Heat Transfer in an Inclined Porous Cavity with Time-Periodic Boundary Conditions

Gang Wang · Qiuwang Wang · Min Zeng · Hiroyuki Ozoe

Received: 4 November 2006 / Accepted: 7 December 2007 / Published online: 8 January 2008

Abstract Kalabin et al. (Numer. Heat Transfer A **47**, 621-631, 2005) studied the unsteady natural convection for the sinusoidal oscillating wall temperature on one side wall and constant average temperature on the opposing side wall. The present article is on the unsteady natural convective heat transfer in an inclined porous cavity with similar temperature boundary conditions as those of Kalabin et al. The inclined angle φ of the cavity is varied from 0° to 80°. The flow field is modeled with the Brinkman-extended Darcy model. The combined effects of inclination angle of the enclosure and oscillation frequency of wall temperature are studied for $Ra^* = 10^3$, $Da = 10^{-3}$, $\varepsilon = 0.6$, and Pr=1. Some results are also obtained with the Darcy–Brinkman–Forchheimer model and Darcy's law and are compared with the present Brinkman-extended Darcy model. The maximal heat transfer rate is attained at the oscillating frequency $f = 46.7\pi$ and the inclined angle $\varphi = 42.2°$.

Keywords Time-periodic boundary conditions · Porous media · Natural convection

Nomenclature

c	Specific heat
c_a	Acceleration coefficient of the porous medium
Da	Darcy number
f	Dimensionless oscillating frequency
F	Inertia coefficient
H	Height of cavity
k	Thermal conductivity

G. Wang · Q. Wang (✉) · M. Zeng · H. Ozoe
State Key Laboratory of Multiphase Flow in Power Engineering, Xi'an Jiaotong University, Xi'an 710049, China
e-mail: wangqw@mail.xjtu.edu.cn

G. Wang
School of Civil Engineering, Lanzhou University of Technology, Lanzhou 730050, China

K Permeability
Nu_{av} Time-averaged Nusselt number in one period
Nu_R Average Nusselt number at right wall
P Dimensionless pressure
p Pressure
Pr Prandtl number
Ra^* Rayleigh–Darcy number
t Time
T Temperature
u, v Velocity components along x- and y-axes, respectively
v Velocity vector
U, V Dimensionless velocity components along X- and Y-axes, respectively
$|V|$ Magnitude of velocity vector
x, y Cartesian coordinates
X, Y Dimensionless Cartesian coordinates

Greek Symbols

α_f Thermal diffusivity
α_m Modified thermal diffusivity of the porous medium
ε Porosity
θ Dimensionless temperature
μ Viscosity
ν_f Fluid kinematic viscosity
ρ Density
τ Dimensionless time
τ_p Dimensionless period of oscillation
σ Specific heat ratio
ω Oscillating frequency
φ Inclined angle of the cavity

Subscripts

f Fluid
m Fluid-saturated porous medium

1 Introduction

Kalabin et al. (2005) recently reported that time-averaged Nusselt number is not zero for an inclined cavity with sinusoidal wall temperature on the one side wall and constant average temperature on the opposing side wall. Their system has no temperature difference between the opposing two side walls in time-averaged sense and there is actually no heat transfer between the walls when these side walls are kept vertically. They found that average Nusselt number takes a maximum value at about an inclined angle $\varphi = 54^\circ$ and dimensionless frequency $f = 20\pi$ for Grashof number $Gr = 2 \times 10^5$ and $Gr = 3 \times 10^5$. The inclined angle φ is measured between the oscillating temperature wall and the vertical gravitational direction. Their finding appears to be striking on the control of natural convection heat transfer rate. They studied cavity flow but similar phenomena may be expected to occur for porous media. This kind of sinusoidal temperature oscillation with net zero temperature difference in time-averaged sense may occur through thermal insulation of building wall and/or

environmental porous ground with temperature oscillation from the ground surface, etc. This is the motivation of the present study.

By the way, Kalabin et al. (2005) made a detailed computation up to inclined angle $\varphi = 89°$, i.e., almost horizontal state of the sinusoidal oscillating temperature. However, for the natural convection in a square enclosure heated from below ($\varphi = 90°$), the preferred mode is multiple roll cells whose axes are horizontal and parallel to the short side axis of the rectangular box. This was mathematically studied by Davis (1967) and subsequently studied experimentally and numerically by a number of reports for horizontal and inclined layers by Hart (1971), and Hollands and Konicek (1973), Ozoe et al. (1974a,b) and for porous layer by Holst and Aziz (1972). For a square cross-sectional enclosure, Ozoe et al. (1974a) experimentally noted a two-dimensional roll cell for the angle of inclination $\varphi < 86°$ or so. According to the experiment by Hollands and Konicek (1973), the longitudinal roll cells (three-dimensional roll cell) exist for most of angles for a shallow layer of width/height = 44. Considering these previous reports, in the present report, the angle of inclination is limited for $\varphi \leq 80°$.

Natural convection heat transfer in a fluid-saturated porous medium has been extensively investigated due to the wide range of geophysical and engineering applications. These include geothermal systems, high-performance building insulation, cooling of electronic devices, and solar power collector, etc. Representative studies in this field have been very well summarized in the recent books by Nield and Bejan (2006), Vafai (2000, 2005), Ingham and Pop (2002), and Pop and Ingham (2001).

In recent years, natural convection in an enclosure with time-periodic thermal boundary conditions has received much attention (Antohe and Lage 1996, 1997; Kwak et al. 1998a,b; Kazmierczak and Chinoda 1992; Lage and Bejan 1993; Kwak and Hyun 1996; Chung et al. 2001). Most of these studies mainly dealt with natural convection of fluid in an enclosure with time-periodic boundary conditions. However, studies of natural convection in a fluid-saturated porous medium system subject to the same boundary conditions are relatively scarce. Some studies on natural convection in a porous cavity with the time-dependent boundary conditions, were made by Antohe and Lage (1994), Kazmierczak and Muley (1994), Chhuon and Caltagirone (1976), and Rudraiah and Malashetty (1990). Meanwhile, it should be noted that, in all the previous studies, the time-averaged temperature of one sidewall was assumed to be higher (or lower) than the constant temperature of the opposite sidewall. Wang et al. (2007a) studied the natural convection of horizontal fluid layer of $Pr = 6$ heated or cooled from one horizontal wall with its temperature oscillated sinusoidally and the opposing horizontal wall kept at the average constant value. They found that the bulk area convection occurs when the lower wall temperature is higher than the upper wall temperature and the temperature-stratified conduction dominance occurs when the upper wall temperature is higher than the lower wall temperature. Due to the combinations of these phenomena, the time-averaged heat flux was found to be always upward in a time-averaged sense even if the time-averaged temperature difference is zero between the top and bottom horizontal walls. They also found this holds even if either top or bottom wall temperature is oscillated. Later, they subsequently studied the similar system for $Pr = 1$ and obtained the similar results (Wang et al. 2007b). On the other hand, Wang et al. (2008) studied the similar geometrical system as that by Kalabin et al. (2005), but for porous layer with positive/negative inclined angles. Even for porous layer, they obtained the similar characteristics of uni-directional heat flux due to the time-dependent dominance of the convection and the conduction.

In the present report, we further study the natural convection in an inclined porous cavity with three different models. Our objective is to find the maximum heat flux at an optimal combination of frequency and inclined angle.

2 Mathematical Formulation

The two-dimensional inclined enclosure under investigation is filled with a fluid-saturated porous medium and all the walls are impermeable. The schematic configuration of the problem is illustrated in Fig. 1, with H denoting the side length of the square enclosure. The fluid is a Newtonian incompressible fluid ($Pr = 1$), and the porous medium is considered to be homogeneous and isotropic. Furthermore, the porous medium is assumed to be in local thermal equilibrium with the fluid. The top and bottom walls of the cavity are adiabatic, and the right sidewall is maintained at a constant temperature T_0. The temperature of the opposing side wall varies sinusoidally in time at about a mean temperature T_0. The thermophysical properties of the fluid and the porous material are taken to be constant except for the density variation in the buoyancy force, which is treated by the Boussinesq approximation.

The Brinkman-extended Darcy formulation, which includes the transport and viscous terms, is adopted for modeling the fluid flow in the porous medium. The governing equations for mass, momentum and energy in two-dimensional, laminar flow are as follows:

$$\nabla \cdot \mathbf{v} = 0 \tag{1}$$

$$\frac{1}{\varepsilon}\frac{\partial \mathbf{v}}{\partial t} + \frac{1}{\varepsilon^2}(\mathbf{v}\cdot\nabla)\mathbf{v} = -\frac{1}{\rho_\mathrm{f}}\nabla p - \frac{\nu_\mathrm{f}}{K}\mathbf{v} + \nu_\mathrm{e}\nabla^2\mathbf{v} - \beta(T - T_0)\mathbf{g} \tag{2}$$

$$(\rho c)_\mathrm{m}\frac{\partial T}{\partial t} + (\rho c)_\mathrm{f}\mathbf{v}\cdot\nabla T = k_\mathrm{m}\nabla^2 T \tag{3}$$

where β is the fluid volumetric expansion coefficient, $\mathbf{g}$ is the gravitational acceleration vector, $\mathbf{v}$ represents the velocity vector, ρ_f is the fluid density, ν_f is the fluid kinematic viscosity, ε and K are the porosity and permeability of porous medium, respectively. T stands for temperature, t for time, k_m is the stagnant thermal conductivity of porous medium, and ν_e is the effective kinematic viscosity of porous medium. The value of ν_f is used as an approximate value of ν_e, i.e., $\nu_\mathrm{e} = \nu_\mathrm{f}$, and this approximation provides good agreement with experimental data obtained by Lundgren (1972).

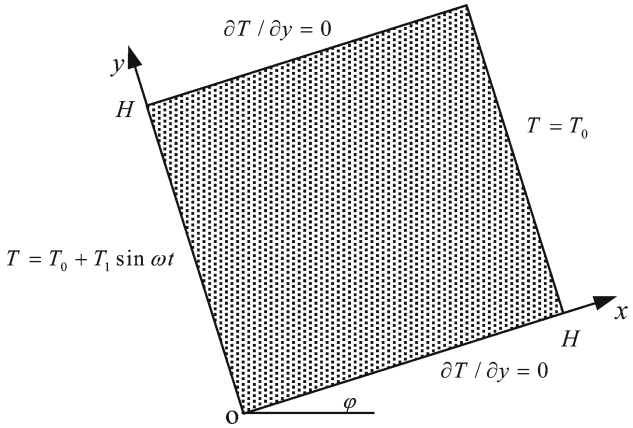

Fig. 1 Physical model and coordinate system

In accordance with the present problem, the governing Eqs. 1–3 are subject to the following initial and boundary conditions:

$$u = v = 0, \quad T = T_0 \quad \text{at } t = 0 \tag{4a}$$

$$u = v = 0, \quad T = T_0 + T_1 \sin \omega t \quad \text{at } x = 0 \tag{4b}$$

$$u = v = 0, \quad T = T_0 \quad \text{at } x = H \tag{4c}$$

$$u = v = 0, \quad \frac{\partial T}{\partial y} = 0 \quad \text{at } y = 0 \text{ and } H. \tag{4d}$$

It can be seen from Eq. 4b that the temperature of the left sidewall oscillates periodically over an average value T_0 with amplitude T_1 and frequency ω.

It is convenient to cast the above governing equations in terms of dimensionless variables such that

$$\begin{gathered} \tau = \frac{t\alpha_{\mathrm{m}}}{\sigma H^2}, \quad X = \frac{x}{H}, \quad Y = \frac{y}{H}, \quad U = \frac{uH}{\alpha_{\mathrm{m}}}, \quad V = \frac{vH}{\alpha_{\mathrm{m}}}, \\ P = \frac{Kp}{\mu\alpha_{\mathrm{m}}}, \quad \theta = \frac{T - T_0}{T_1}, \quad Pr = \frac{\nu_{\mathrm{f}}}{\alpha_{\mathrm{m}}}, \quad Da = \frac{K}{H^2} \end{gathered} \tag{5}$$

where Pr and Da are the Prandtl number and the Darcy number, respectively. α_{m} is the modified thermal diffusivity defined as $k_{\mathrm{m}}/(\rho c)_{\mathrm{f}}$. Upon employing the dimensionless variables, the governing Eqs. 1–3 can be non-dimensionalized as follows:

$$\frac{\partial U}{\partial X} + \frac{\partial V}{\partial Y} = 0 \tag{6}$$

$$\frac{Da}{Pr}\left[\frac{1}{\varepsilon\sigma}\frac{\partial U}{\partial \tau} + \frac{1}{\varepsilon^2}\left(U\frac{\partial U}{\partial X} + V\frac{\partial U}{\partial Y}\right)\right] = -\frac{\partial P}{\partial X} + Da\nabla^2 U - U + Ra^*\theta \sin\varphi \tag{7}$$

$$\frac{Da}{Pr}\left[\frac{1}{\varepsilon\sigma}\frac{\partial V}{\partial \tau} + \frac{1}{\varepsilon^2}\left(U\frac{\partial V}{\partial X} + V\frac{\partial V}{\partial Y}\right)\right] = -\frac{\partial P}{\partial Y} + Da\nabla^2 V - V + Ra^*\theta \cos\varphi \tag{8}$$

$$\frac{\partial \theta}{\partial \tau} + U\frac{\partial \theta}{\partial X} + V\frac{\partial \theta}{\partial Y} = \nabla^2\theta \tag{9}$$

where φ is the inclined angle of the cavity. The heat capacity ratio σ and Rayleigh–Darcy number Ra^* are defined as

$$\sigma = \frac{(\rho c)_{\mathrm{m}}}{(\rho c)_{\mathrm{f}}}, \quad Ra^* = \frac{gK\beta T_1 H}{\nu_{\mathrm{f}}\alpha_{\mathrm{m}}}. \tag{10}$$

The corresponding dimensionless initial and boundary conditions are given by

$$U = V = 0, \quad \theta = 0 \quad \text{at } \tau = 0 \tag{11a}$$

$$U = V = 0, \quad \theta = \sin f\tau \quad \text{at } X = 0 \tag{11b}$$

$$U = V = 0, \quad \theta = 0 \quad \text{at } X = 1 \tag{11c}$$

$$U = V = 0, \quad \frac{\partial \theta}{\partial Y} = 0 \quad \text{at } Y = 0 \text{ and } 1 \tag{11d}$$

where f is the dimensionless oscillating frequency of the boundary temperature and is defined as

$$f = \frac{\omega \sigma H^2}{\alpha_m} \tag{12}$$

The dimensionless period of the temperature oscillation, τ_p, can be expressed as follows

$$\tau_p = \frac{2\pi}{f}. \tag{13}$$

3 Numerical Method

The dimensionless governing Eqs. 6–9 have been solved using the control volume procedure outlined by Patankar (1980). The SIMPLER algorithm is employed to couple the velocities and pressure. The control volume formulation utilized in this algorithm ensures conservation of momentum and energy as well as the continuity of fluxes. The harmonic mean formulation selected for the interface diffusion coefficients between two control volumes can handle abrupt changes in these coefficients. A fully implicit scheme is applied for discretizing the time derivatives. The convective terms are discretized by using the QUICK scheme reported by Hayase et al. (1992), and a second-order central difference scheme is used for the diffusion terms. The resulting algebraic equations are solved by the tri-diagonal matrix algorithm (TDMA).

A grid independent test was performed using three sets of grids: 31×31, 51×51, and 81×81. The results showed insignificant differences between the 51×51 and 81×81 grids. Therefore, for all computations in this paper, a $51(X) \times 51(Y)$ staggered, non-uniform grid was employed. Grid stretching was made to cluster the mesh points near the boundary walls where sharp gradients of velocity and temperature are expected. For each time step during the computations, the convergence of computations is declared when the maximum relative changes in the variables (U, V, θ) between two successive iterations are less than 10^{-6}. To validate the computer code, the previously published problems on natural convection in a differentially heated cavity, filled with a fluid-saturated medium, were solved. As shown in Table 1, the average Nusselt numbers are in good agreement with the Darcy–Brinkman solutions reported by Lauriat and Prasad (1989). These comprehensive verification efforts demonstrated the robustness and accuracy of the present numerical method.

Table 1 Comparison of average Nusselt number predictions with the computed data of Lauriat and Prasad (1989) ($Pr = 1$)

No.	Ra^*	Da	ε	Nu	
				Present	Lauriat and Prasad (1989)
1	10^4	10^{-4}	0.4	25.75	25.70
2	10^2	10^{-6}	0.4	3.102	3.06
3	10	10^{-6}	0.1	1.073	1.07
4	10^3	10^{-6}	0.4	13.34	13.22
5	10	10^{-2}	0.4	1.02	1.02

4 Results and Discussion

In order to mainly investigate the effects of the inclined angle and oscillating frequency on natural convection, the Rayleigh–Darcy, Darcy and Prandtl numbers, porosity, and heat capacity ratio were kept constant: $Ra^* = 10^3$, $Da = 10^{-3}$, $Pr = 1$, $\varepsilon = 0.6$, and $\sigma = 1$. In this investigation, the time step is $\Delta\tau = 5 \times 10^{-6}$. In order to obtain a periodic oscillating solution independent of initial state, 5–10 oscillating periods were needed to be calculated. Based on the above given conditions, numerical results were obtained for the values of the inclined angle $0° \le \varphi \le 80°$ and various values of the dimensionless oscillating frequency.

4.1 Representative Temperature and Flow Fields

Figures 2 and 3 present the time-dependent flow patterns and isotherms over the duration of the 10th period for $f = 40\pi$ and $\varphi = 45°$ at $Ra^* = 10^3$, $Da = 10^{-3}$, $Pr = 1$, and $\varepsilon = 0.6$. The parameter $\tau_p(\tau_p = 2\pi/f)$ stands for the dimensionless period of the temperature oscillation and is 0.05 at $f = 40\pi$. The solid lines indicate the positive contour values while the dashed lines the negative contour values. The subplots (a)–(h) show the corresponding seven phases from $\tau = 0.45$ to 0.49375 with $\Delta\tau = \tau_p/8$ (the 10th fully developed period). It can be found that the flow field transition is quite complicated in one period. At $\tau = 0.45$, we can see from Fig. 2a that there are two clockwise circulations in the lower and upper regions of the cavity and a counterclockwise circulation containing two cells appears between the two clockwise circulations. As the dimensionless time increases, a single roll cell of clockwise circulation occupies the entire cavity at $\tau = 0.4625$, 0.46875, and 0.475. At these instants, the left sidewall temperature is higher than or equal to the constant temperature of the right sidewall and the buoyancy force induces the clockwise convection in a whole cross section. On the other hand, at $\tau = 0.48125$, 0.4875, and 0.49375, the left sidewall temperature is lower than the constant temperature of the right sidewall and the buoyancy force induces the anti-clockwise convection. This anti-clockwise convection works only along the left sidewall and is limited in the lower half region in contrast to the previous clockwise convection. Because of this reason, there are two circulations with different directions of rotation in the cavity for these latter instants. The boundary layer like upward flow can be seen from Fig. 3 near the heated left sidewall. This bulk convection is changed to the downward boundary layer like flow at (e) $\tau = 0.475$ or after.

4.2 Effect of the Inclined Angle on Heat Transfer Rates at a Given Oscillating Frequency

The average Nusselt number along the right sidewall ($X = 1$) is defined as

$$Nu_R = -\int_0^1 \left.\frac{\partial\theta}{\partial X}\right|_{X=1} dY \tag{14}$$

The periodic oscillations of Nu_R at $f = 20\pi$, $Ra^* = 10^3$, $Da = 10^{-3}$, $Pr = 1$, and $\varepsilon = 0.6$ are shown in Fig. 4 for $\varphi = 0°$, 45°, and 80°.

It can be shown that the Nusselt number Nu_R at $\varphi = 0°$ varies with the identical values of the positive and negative amplitudes to indicate the net zero heat flux from the oscillating temperature wall to the constant temperature wall. As the inclined angle increases, the Nusselt number becomes larger than zero when it is integrated in time. This suggests that the heat flux is positive from the left sidewall to the right sidewall in spite of the net zero temperature difference between these two walls in a time-averaged sense. In order to check this behavior, further computations are made to obtain the periodic oscillations of Nu_R at

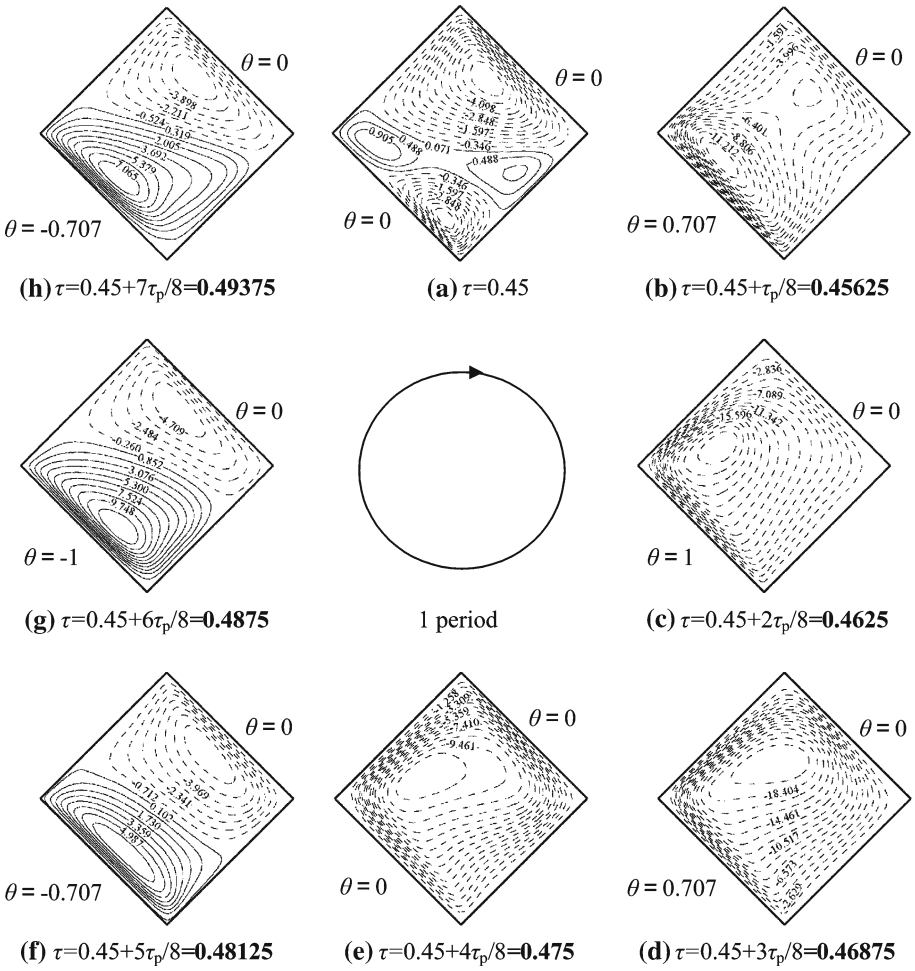

Fig. 2 Sequential plots of stream functions during one period for $f = 40\pi$ and $\varphi = 45°$ at $Ra^* = 10^3$, $Da = 10^{-3}$, $Pr = 1$, and $\varepsilon = 0.6$. (**a**) $\tau = 0.45$; (**b**) $\tau = 0.45 + \tau_p/8 = 0.45625$; (**c**) $\tau = 0.45 + 2\tau_p/8 = 0.4625$; (**d**) $\tau = 0.45 + 3\tau_p/8 = 0.46875$; (**e**) $\tau = 0.45 + 4\tau_p/8 = 0.475$; (**f**) $\tau = 0.45 + 5\tau_p/8 = 0.48125$; (**g**) $\tau = 0.45 + 6\tau_p/8 = 0.4875$; (**h**) $\tau = 0.45 + 7\tau_p/8 = 0.49375$

$f = 20\pi$, $Ra^* = 10^2$ and 3×10^3, $Da = 10^{-3}$, $Pr = 1$, and $\varepsilon = 0.6$ for $\varphi = 0°, 45°$ and 80°. As shown in Figs. 5 and 6, the basic behavior at different Rayleigh–Darcy number is the same. This agrees with the results for fluid layer studied by Kalabin et al. (2005).

4.3 Effect of the Oscillating Frequency on Heat Transfer Rates at a Given Inclined Angle

Figure 7 shows the periodic oscillations of Nu_R at $\varphi = 45°$, $Ra^* = 10^3$, $Da = 10^{-3}$, $Pr = 1$, and $\varepsilon = 0.6$ and for $f = 5\pi, 40\pi, 160\pi$, and 320π. This figure clearly shows that the amplitude of Nusselt number decreases with the increase in the oscillating frequency. As the frequency increases to 320π, the Nusselt number changes only slightly and approaches to a constant value. When the oscillating frequency increases, the temperature oscillation of the left sidewall does not affect the temperature of the interior fluid region in the cavity quickly.

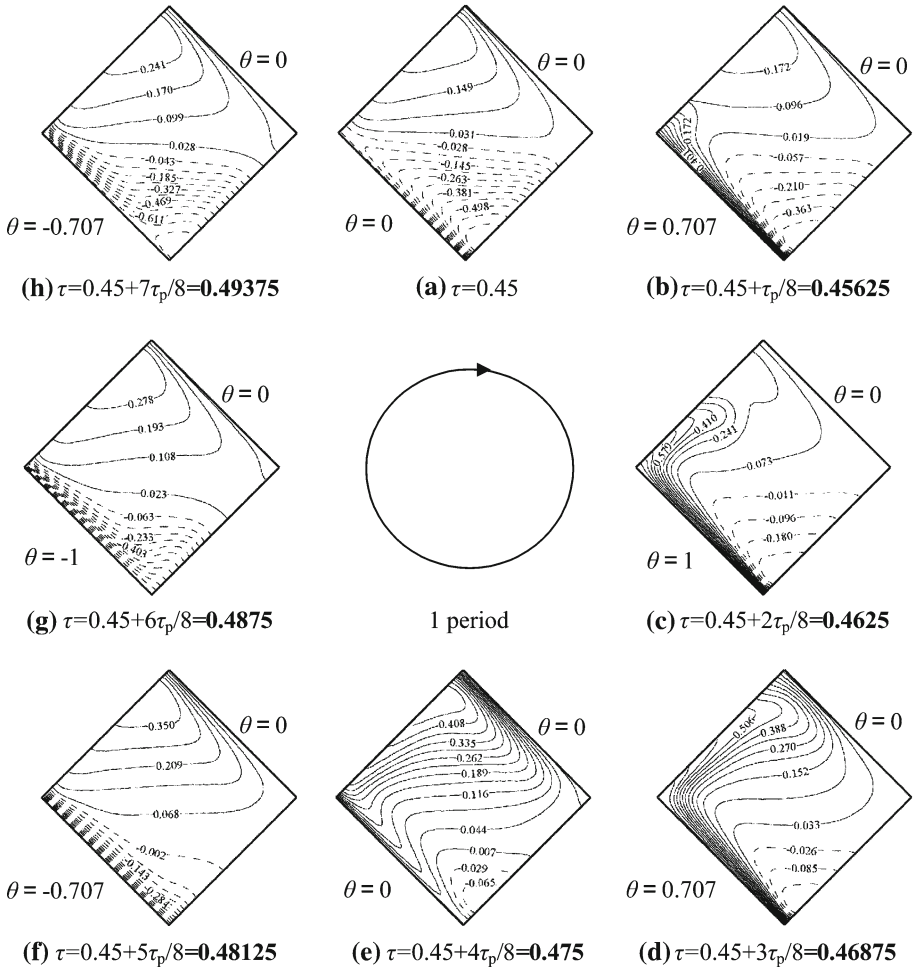

(h) τ=0.45+7τ_p/8=**0.49375** **(a)** τ=0.45 **(b)** τ=0.45+τ_p/8=**0.45625**

(g) τ=0.45+6τ_p/8=**0.4875** 1 period **(c)** τ=0.45+2τ_p/8=**0.4625**

(f) τ=0.45+5τ_p/8=**0.48125** **(e)** τ=0.45+4τ_p/8=**0.475** **(d)** τ=0.45+3τ_p/8=**0.46875**

Fig. 3 Sequential plots of isotherms during one period for $f = 40\pi$ and $\varphi = 45°$ at $Ra^* = 10^3$, $Da = 10^{-3}$, $Pr = 1$, and $\varepsilon = 0.6$. (**a**) $\tau = 0.45$; (**b**) $\tau = 0.45 + \tau_p/8 = 0.45625$; (**c**) $\tau = 0.45 + 2\tau_p/8 = 0.4625$; (**d**) $\tau = 0.45 + 3\tau_p/8 = 0.46875$; (**e**) $\tau = 0.45 + 4\tau_p/8 = 0.475$; (**f**) $\tau = 0.45 + 5\tau_p/8 = 0.48125$; (**g**) $\tau = 0.45 + 6\tau_p/8 = 0.4875$; (**h**) $\tau = 0.45 + 7\tau_p/8 = 0.49375$

The heat transfer rate converges to a constant value as the oscillating frequency approaches infinity ($f \to \infty$).

4.4 The Time-Averaged Nusselt Number for One Period

The time-averaged Nusselt number along the right sidewall (X=1) is defined as:

$$Nu_{av} = -\frac{f}{2\pi}\int_0^{2\pi/f}\int_0^1 \left.\frac{\partial\theta}{\partial X}\right|_{X=1} \mathrm{d}Y\,\mathrm{d}\tau \tag{15}$$

Figure 8 presents the variation of Nu_{av} with the oscillating frequency f for $\varphi = 45°$ and 50° at $Ra^* = 10^3$, $Da = 10^{-3}$, $Pr = 1$, and $\varepsilon = 0.6$. As shown in Fig. 8, the oscillating frequency f varies from 5π to 200π and its increasing interval Δf is set to be 5π. The time-

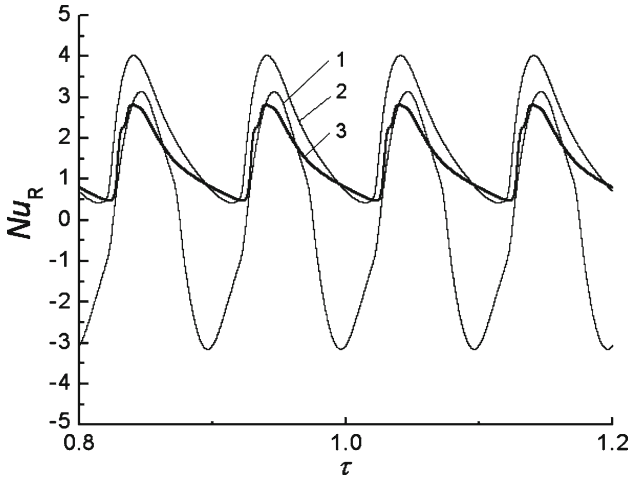

Fig. 4 Time-dependent behavior of the Nusselt number at the right sidewall ($X = 1$) for $f = 20\pi$ and various values of φ. 1. $\varphi = 0°$; 2. $\varphi = 45°$; 3. $\varphi = 80°$ at $Ra^* = 10^3$, $Da = 10^{-3}$, $Pr = 1$, and $\varepsilon = 0.6$

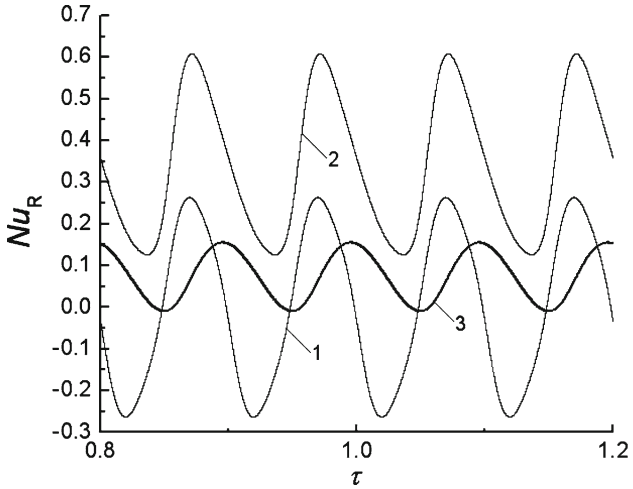

Fig. 5 Time-dependent behavior of the Nusselt number at the right sidewall ($X = 1$) for $f = 20\pi$ and various values of φ. 1. $\varphi = 0°$; 2. $\varphi = 45°$; 3. $\varphi = 80°$ at $Ra^* = 10^2$, $Da = 10^{-3}$, $Pr = 1$, and $\varepsilon = 0.6$

averaged Nusselt number reaches a maximum value at about $f = 40\pi \sim 50\pi$, and decreases with the oscillating frequency increasing further. When $f = 200\pi$, the time-averaged Nusselt number approaches unity. Figure 9 depicts the variation of Nu_{av} with the inclined angle for $f = 40\pi$ and 50π at $Ra^* = 10^3$, $Da = 10^{-3}$, $Pr = 1$, and $\varepsilon = 0.6$. The inclined angle φ varies from 0° to 80°, whose increasing interval $\Delta\varphi$ is 5°. From this figure, we can see that the time-averaged Nusselt number reaches a maximum value at $\varphi = 40° \sim 45°$ for $f = 40\pi$ and 50π. It can be concluded from Figs. 8 and 9 that there exists a maximum value of time-averaged Nusselt number for an optimal combination of frequency and angle of inclination. In order to obtain this maximum Nu point, we did computations using trial and error approach with increments of 0.1° and 0.1π in φ and f, respectively. As shown in Table 2,

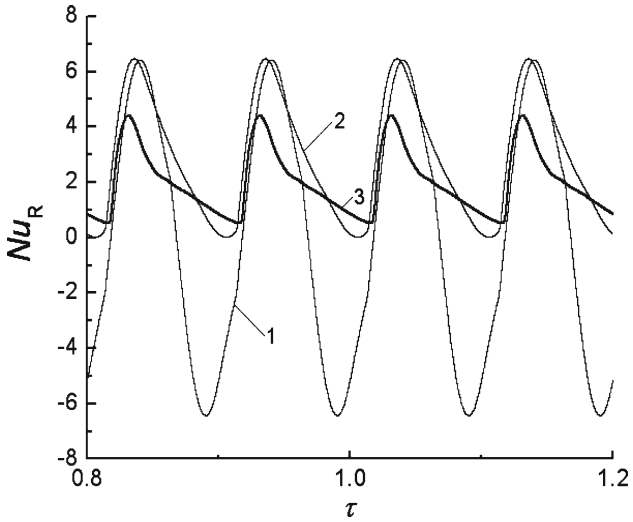

Fig. 6 Time-dependent behavior of the Nusselt number at the right sidewall ($X = 1$) for $f = 20\pi$ and various values of φ. 1.$\varphi = 0°$; 2. $\varphi = 45°$; 3. $\varphi = 80°$ at $Ra^* = 3 \times 10^3$, $Da = 10^{-3}$, $Pr = 1$, and $\varepsilon = 0.6$

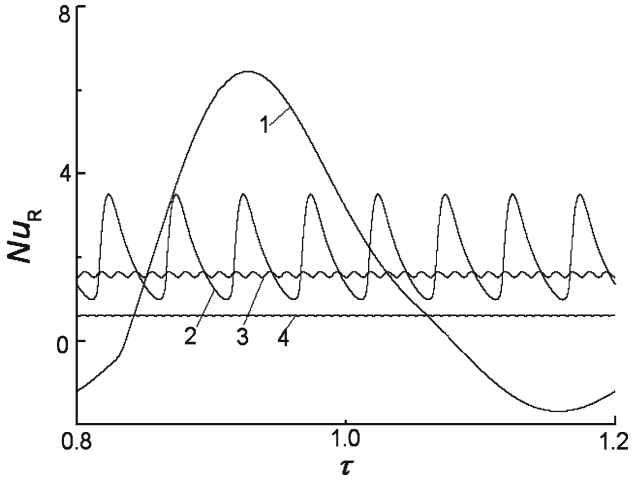

Fig. 7 Time-dependent behavior of the Nusselt number at the right sidewall ($X = 1$) for $\varphi = 45°$ and various values of f. 1. $f = 5\pi$; 2. $f = 40\pi$; 3. $f = 160\pi$; 4. $f = 320\pi$ at $Ra^* = 10^3$, $Da = 10^{-3}$, $Pr = 1$, and $\varepsilon = 0.6$

the maximum value of time-averaged Nusselt number exists in the range $f = 40\pi \sim 50\pi$ at $\varphi = 40° \sim 45°$. From Table 2, we can see that the time-averaged Nusselt number reaches the maximum value of 2.022242 at $f = 46.7\pi$ and $\varphi = 42.2°$.

4.5 Some Results for $f = 20\pi$ Using the Darcy–Brinkman–Forchheimer Model and Darcy's Law

In order to check the computed results for different models, we also employ the Darcy–Brinkman–Forchheimer (DBF) model and Darcy's law rather than the above Brinkman-

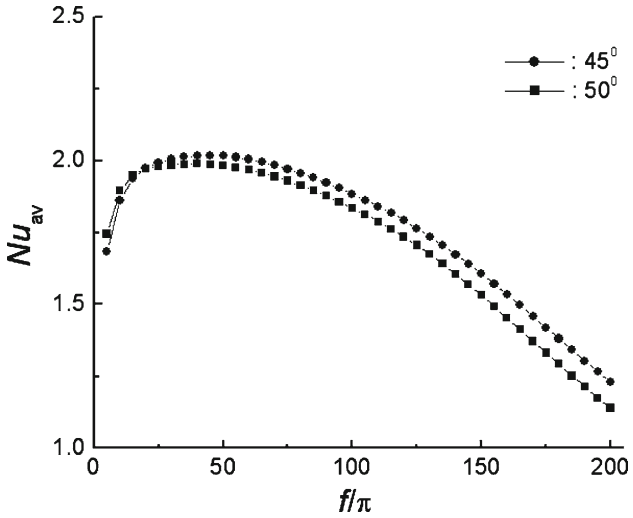

Fig. 8 Variation of Nu_{av} with f for $\varphi = 45°$ and $\varphi = 50°$ at $Ra^* = 10^3$, $Da = 10^{-3}$, $Pr = 1$, and $\varepsilon = 0.6$

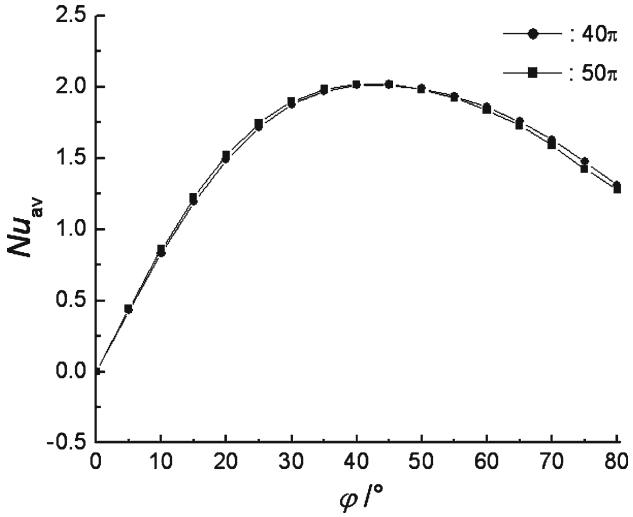

Fig. 9 Variation of Nu_{av} with φ for $f = 40\pi$ and 50π at $Ra^* = 10^3$, $Da = 10^{-3}$, $Pr = 1$, and $\varepsilon = 0.6$

extended Darcy (BD) model to solve the present problem and some of the results are described as follows.

Based on the work by Nithiarasu et al. (1997, 1999), the dimensionless momentum equations for DBF model are:

$$\frac{Da}{Pr}\left[\frac{1}{\varepsilon\sigma}\frac{\partial U}{\partial \tau}+\frac{1}{\varepsilon^2}(\mathbf{V}\cdot\nabla U)\right]=-\frac{\partial P}{\partial X}-U+\frac{Da}{\varepsilon}\nabla^2 U-\frac{F\sqrt{Da}}{Pr}|\mathbf{V}|\,U+Ra^*\theta\sin\varphi \tag{16}$$

Table 2 Time-averaged Nu at some different frequencies and inclined angles at $Ra^* = 10^3$, $Da = 10^{-3}$, $Pr = 1$, and $\varepsilon = 0.6$

f	Nu_{av}									
	$\varphi = 40°$	$\varphi = 41°$	$\varphi = 42°$	$\varphi = 42.1°$	$\varphi = 42.2°$	$\varphi = 42.3°$	$\varphi = 42.4°$	$\varphi = 43°$	$\varphi = 44°$	$\varphi = 45°$
40π	2.01374	2.01702	2.01881	2.01891	2.01900	2.01907	2.01913	2.01920	2.01827	2.01609
43π	2.01694	2.01977	2.02114	2.02120	2.02125	2.02128	2.02130	2.02114	2.01983	2.01729
44π	2.01767	2.02037	2.02161	2.02166	2.02170	2.02172	2.02173	2.02149	2.02007	2.01742
45π	2.01825	2.02082	2.02195	2.02199	2.02201	2.02202	2.02202	2.02172	2.02020	2.01745
46π	2.01867	2.02113	2.02215	2.022173	2.022186	2.022185	2.022170	2.02181	2.02019	2.01734
46.1π	2.01871	2.02115	2.02216	2.022183	2.022194	2.022193	2.022178	2.02181	2.02018	2.01732
46.2π	2.01874	2.02117	2.02217	2.022192	2.022203	2.022200	2.022184	2.02181	2.02017	2.01730
46.3π	2.01877	2.02119	2.02218	2.022199	2.022209	2.022205	2.022188	2.02181	2.02016	2.01728
46.4π	2.01882	2.02123	2.02220	2.022226	2.022235	2.022231	2.022212	2.02183	2.02017	2.01728
46.5π	2.01885	2.02124	2.02221	2.022231	2.022239	2.022233	2.022214	2.02182	2.02015	2.01726
46.6π	2.01887	2.02126	2.02221	2.022234	2.022240	2.022234	2.022214	2.02182	2.02014	2.01723
46.7π	2.01890	2.02127	2.02222	2.022236	2.022242	2.022234	2.022213	2.02181	2.02012	2.01721
46.8π	2.01892	2.02128	2.02222	2.022236	2.022241	2.022232	2.022210	2.02180	2.02010	2.01718
46.9π	2.01894	2.02129	2.02222	2.022235	2.022239	2.022230	2.022206	2.02179	2.02008	2.01715
47π	2.01896	2.02130	2.02222	2.022233	2.022235	2.022224	2.022200	2.02178	2.02006	2.01712
48π	2.01910	2.02133	2.02215	2.02215	2.02215	2.02212	2.02209	2.02162	2.01981	2.01678
50π	2.01896	2.02099	2.02162	2.02161	2.02159	2.02155	2.02150	2.02092	2.01894	2.01574

$$\frac{Da}{Pr}\left[\frac{1}{\varepsilon\sigma}\frac{\partial V}{\partial \tau}+\frac{1}{\varepsilon^2}(\mathbf{V}\cdot\nabla V)\right]=-\frac{\partial P}{\partial Y}-V+\frac{Da}{\varepsilon}\nabla^2 V-\frac{F\sqrt{Da}}{Pr}|\mathbf{V}|\,V+Ra^*\theta\cos\varphi \tag{17}$$

where F is the inertia coefficient and $F = 1.75(150\varepsilon^3)^{-0.5}$ according to the Ergun's correlation (1952), and $|\mathbf{V}|$ is the magnitude of the dimensionless velocity vector and $|\mathbf{V}| = \sqrt{U^2+V^2}$. The dimensionless energy equation and boundary conditions are the same as those given in Sect. 2.

Figure 10 shows the periodic oscillations of Nu_R at $f = 20\pi$, $Ra^* = 10^3$, $Da = 10^{-3}$, $Pr = 1$, and $\varepsilon = 0.6$ for $\varphi = 0°$, 45°, and 80° using the above DBF model. Comparing the results between Fig. 10 (DBF model) and Fig. 4 (BD model), we can see that the general behavior of Nu_R is quite similar, though the amplitude of Nu_R curve by the DBF model is slightly smaller than those by BD model. This is due to the DBF model includes a quadratic drag term.

The dimensionless momentum equations for Darcy's law are as follows following Nield and Bejan (2006),

$$\frac{c_a Da}{\sigma Pr}\frac{\partial U}{\partial \tau}=-\frac{\partial P}{\partial X}-U+Ra^*\theta\sin\varphi \tag{18}$$

$$\frac{c_a Da}{\sigma Pr}\frac{\partial V}{\partial \tau}=-\frac{\partial P}{\partial Y}-V+Ra^*\theta\cos\varphi \tag{19}$$

where c_a is the acceleration coefficient of the porous medium and let $c_a = 1$ during the computation. The other equations are also the same as those given in Sect. 2. The dimensionless boundary conditions become with the slip boundary conditions described in the book edited by Vafai (2000).

$$U = V = 0, \quad \theta = 0 \quad \text{at } \tau = 0 \tag{20a}$$

$$U = 0, \quad \theta = \sin f\tau \quad \text{at } X = 0 \tag{20b}$$

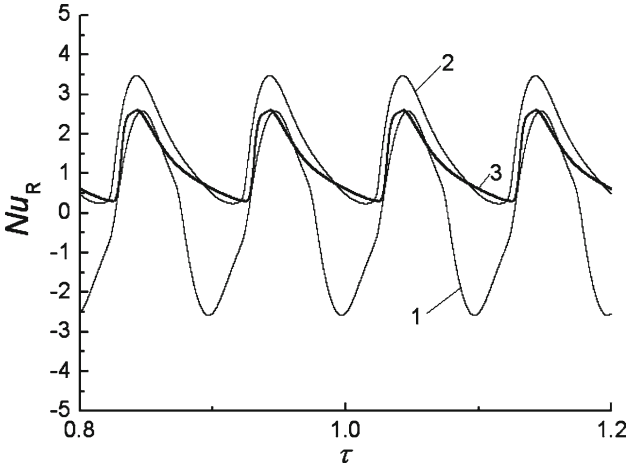

Fig. 10 Time-dependent behavior of the Nusselt number at the right sidewall ($X = 1$) for $f = 20\pi$ and various values of φ. 1. $\varphi = 0°$; 2. $\varphi = 45°$; 3. $\varphi = 80°$ (DBF model) at $Ra^* = 10^3$, $Da = 10^{-3}$, $Pr = 1$, and $\varepsilon = 0.6$

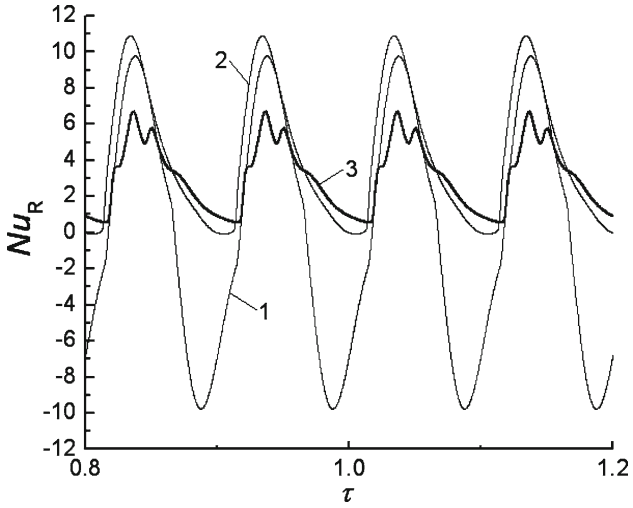

Fig. 11 Time-dependent behavior of the Nusselt number at the right sidewall ($X = 1$) for $f = 20\pi$ and various values of φ. 1. $\varphi = 0°$; 2. $\varphi = 45°$; 3. $\varphi = 80°$ (Darcy's law) at $Ra^* = 10^3$, $Da = 10^{-3}$, $Pr = 1$, and $\varepsilon = 0.6$

$$U = 0, \quad \theta = 0 \quad \text{at } X = 1 \tag{20c}$$

$$V = 0, \quad \frac{\partial \theta}{\partial Y} = 0 \quad \text{at } Y = 0 \text{ and } 1 \tag{20d}$$

Figure 11 presents the time-dependent oscillations of Nu_R at $f = 20\pi$, $Ra^* = 10^3$, $Da = 10^{-3}$, $Pr = 1$, and $\varepsilon = 0.6$ for $\varphi = 0°$, 45°, and 80° using Darcy's law. Comparing the results between Fig. 11 (Darcy's law) and Fig. 4 (BD model), we can see that the oscillation period and general behavior of Nu_R are basically similar, though the amplitude of Nu_R curve by Darcy's law is larger than those by BD model. This would be because, the viscous drag force (the Brinkman term) is neglected when Darcy's law is used.

5 Conclusions

A numerical study of laminar natural convection in an inclined porous cavity with time-periodic boundary conditions is performed. The effects of the inclined angle of the cavity and the dimensionless oscillating frequency on hydrodynamic and heat transfer characteristics are investigated.

Numerical results indicate that there exist an optimum oscillating frequency and an inclined angle, which make the time-averaged Nusselt number of the right sidewall reach a maximum value. For the parameters in the present study, the corresponding maximal time-averaged Nusselt number of the right sidewall can be acquired at $f = 46.7\pi$ and $\varphi = 42.2°$. It is found that the oscillating temperature of the left sidewall has little effect on the temperature in the region near the right sidewall when the inclined angle is maintained at a fixed value and the oscillating frequency approaches infinity. These characteristics in porous media are similar to those reported by Kalabin et al. (2005) for inclined fluid layer.

Acknowledgements We would like to acknowledge financial support for this work provided by the National Natural Science Foundation of China (No. 50521604).

References

Antohe, B.V., Lage, J.L.: A dynamic thermal insulator: inducing resonance within a fluid saturated porous medium enclosure heated periodically from the side. Int. J. Heat Mass Transfer **37**, 771–782 (1994)

Antohe, B.V., Lage, J.L.: Amplitude effects on convection induced by time-periodic horizontal heating. Int. J. Heat Mass Transfer **38**, 1121–1133 (1996)

Antohe, B.V., Lage, J.L.: The Prandtl number effect on the optimum heating frequency of an enclosure filled with fluid or with a saturated porous medium. Int. J. Heat Mass Transfer **40**, 1313–1323 (1997)

Chhuon, B., Caltagirone, J.P.: Stability of a horizontal porous layer with timewise periodic boundary conditions. ASME J. Heat Transfer **98**, 49–54 (1976)

Chung, K.H., Kwak, H.S., Hyun, J.M.: Finite-wall effect on buoyant convection in an enclosure with pulsating exterior surface temperature. Int. J. Heat Mass Transfer **44**, 721–732 (2001)

Davis, S.H.: Convection in a box: linear theory. J. Fluid Mech. **30**, 465–478 (1967)

Ergun, S.: Fluid flow through packed columns. Chem. Eng. Prog. **48**, 89–94 (1952)

Hart, J.E.: Stability of flow in a differentially heated inclined box. J. Fluid Mech. **47**, 547–576 (1971)

Hayase, T., Humphrey, J.A.C., Greif, R.: A consistently formulated QUICK scheme for fast and stable convergence using finite-volume calculation procedures. J. Comput. Phys. **98**, 108–118 (1992)

Hollands, K.G.T., Konicek, L.: Experimental study of the stability of differentially heated inclined air layers. Int. J. Heat Mass Transfer **16**, 1467–1476 (1973)

Holst, P.H., Aziz, K.: A theoretical and experimental study of natural convection in a confined porous medium. Can. J. Chem. Eng. **50**, 232–241 (1972)

Ingham, D.B., Pop, I. (eds.): Transport Phenomena in Porous Media, vol 2. Pergamon, Oxford (2002)

Kalabin, E.V., Kanashina, M.V., Zubkov, P.T.: Natural-convection heat transfer in a square cavity with time-varying side-wall temperature. Numer. Heat Transfer A **47**, 621–631 (2005)

Kazmierczak, M., Chinoda, Z.: Buoyancy-driven flow in an enclosure with time periodic boundary conditions. Int. J. Heat Mass Transfer **35**, 1507–1518 (1992)

Kazmierczak, M., Muley, A.: Steady and transient natural convection experiments in a horizontal porous layer: the effects of a thin top fluid layer and oscillating bottom wall temperature. Int. J. Heat Fluid Flow **15**, 30–41 (1994)

Kwak, H.S., Hyun, J.M.: Natural convection in an enclosure having a vertical sidewall with time-varying temperature. J. Fluid Mech. **329**, 65–88 (1996)

Kwak, H.S., Kuwahara, K., Hyun, J.M.: Resonant enhancement of natural convection heat transfer in a square enclosure. Int. J. Heat Mass Transfer **41**, 2837–2846 (1998a)

Kwak, H.S., Kuwahara, K., Hyun, J.M.: Prediction of the resonance frequency of natural convection in an enclosure with time-periodic heating imposed on one sidewall. Int. J. Heat Mass Transfer **41**, 3157–3160 (1998b)

Lage, J.L., Bejan, A.: The resonance of natural convection in an enclosure heated periodically from the side. Int. J. Heat Mass Transfer **36**, 2027–2038 (1993)

Lauriat, G., Prasad, V.: Non-Darcian effects on natural convection in a vertical porous enclosure. Int. J. Heat Mass Transfer **32**, 2135–2148 (1989)

Lundgren, T.S.: Slow flow through stationary random beds and suspensions of spheres. J. Fluid Mech. **51**, 273–299 (1972)

Nield, D.A., Bejan, A.: Convection in Porous Media, 3rd edn. Springer, New York (2006)

Nithiarasu, P., Seetharamu, K.N., Sundararajan, T.: Natural convective heat transfer in a fluid saturated variable porosity medium. Int. J. Heat Mass Transfer **40**, 3955–3967 (1997)

Nithiarasu, P., Seetharamu, K.N., Sundararajan, T.: Numerical investigation of buoyancy driven flow in a fluid saturated non-Darcian porous medium. Int. J. Heat Mass Transfer **42**, 1205–1215 (1999)

Ozoe, H., Sayama, H., Churchill, S.W.: Natural convection in an inclined square channel. Int. J. Heat Mass Transfer **17**, 401–406 (1974a)

Ozoe, H., Yamamoto, K., Sayama, H., Churchill, S.W.: Natural circulation in an inclined rectangular channel heated on one side and cooled on the opposing side. Int. J. Heat Mass Transfer **17**, 1209–1217 (1974b)

Patankar, S.V.: Numerical Heat Transfer and Fluid Flow. McGraw-Hill, New York (1980)

Pop, I., Ingham, D.B.: Convective Heat Transfer: Mathematical and Computational Modelling of Viscous Fluids and Porous Media. Oxford, Pergamon (2001)

Rudraiah, N., Malashetty, M.S.: Effect of modulation on the onset of convection in sparsely packed porous layer. ASME J. Heat Transfer **112**, 685–689 (1990)

Vafai, K. (ed.): Handbook of Porous Media. Marcel Dekker, New York (2000)
Vafai, K. (ed.): Handbook of Porous Media. 2nd edn. Taylor & Francis, Baton Rouge (2005)
Wang, Q.W., Wang, G., Zeng, M., Ozoe, H.: Upward heat flux through the horizontal fluid layer of water with sinusoidal wall temperature at the top or bottom boundary. Numer. Heat Transfer A **52**, 817–829 (2007a)
Wang, Q.W., Wang, G., Zeng, M., Ozoe H.: Uni-directional heat flux through the horizontal fluid layer with sinusoidal wall temperature at the top or bottom boundaries. Int. J. Heat Mass Transfer (2007b). doi: 10.1016/j.ijheatmasstransfer.2007.07.030
Wang, G., Wang, Q.W., Zeng, M., Ozoe, H.: Natural convection heat transfer in an inclined porous cavity under time-periodic boundary conditions with positive/negative inclined angles. J. Porous Media (2008, in press)